RSC Advances

PAPER

View Article Online
View Journal | View Issue

Cite this: *RSC Adv.*, 2024, **14**, 37438

Rapid activation of a solution-processed aluminum oxide gate dielectric through intense pulsed light irradiation

Yeon-Wha Oh,[ab] Hoon Kim,[c] Lee-Mi Do,[c] Kyu-Ha Baek,[c] Il-Suk Kang,[a] Ga-Won Lee*[b] and Chan-mo Kang*[c]

In this study, we report rapid activation of a solution-processed aluminum oxide gate dielectric film to reduce its processing time under ambient atmosphere. Aluminum precursor films were exposed to a high energy light-pulse and completely converted into dielectric films within 30 seconds (450 pulses). The aluminum oxide gate dielectric film irradiated using intense pulsed light with 450 pulses exhibits a smooth surface and a leakage current density of less than 10^{-8} A cm^{-2} at 2 MV cm^{-1}. Moreover, dielectric constants of the aluminum oxide layer were calculated to be approximately 7. Finally, we fabricated a solution-processed indium gallium zinc oxide thin-film transistor with AlO_x using intense pulsed light irradiation, exhibiting a field-effect mobility of 2.99 cm^2 V^{-1} s^{-1}, threshold voltage of 0.73 V, subthreshold swing of 180 mV per decade and I_{on}/I_{off} ratio of 3.9×10^6.

Received 23rd September 2024
Accepted 7th November 2024

DOI: 10.1039/d4ra06855f

rsc.li/rsc-advances

Introduction

Metal oxide thin-film transistors (TFTs) represent a new era of display applications because of their high transparency, large-area uniformity, and high mobility.[1–3] In particular, metal oxide materials can be applied in TFTs as semiconductors, transparent electrodes, and insulators.[4–9] Among these, insulators play an important role in TFTs because they determine the breakdown voltage, leakage current, and charge accumulation at the dielectric/semiconductor interface.[10] Silicon dioxide (SiO_2) has mainly been adopted as a gate insulator in oxide TFTs, but various high dielectric constant (high-κ) materials such as yttrium trioxide, zirconium oxide (ZrO_2), hafnium dioxide, and aluminum oxide (AlO_x) have recently been researched to reduce leakage currents and achieve high capacitance.[11–17]

High-κ gate dielectric films must have smooth surfaces and dense structures to achieve low leakage current, stable operation, and high breakdown voltage. Among these, aluminum oxide is the most attractive material because of its low interface trap density with oxide semiconductors, high breakdown field, and smooth surface. Generally, AlO_x is deposited using vacuum-based processes such as atomic layer deposition, chemical vapor deposition, and sputtering; however, these methods have been limited by the lack of low-cost devices. A simple solution process, which converts a metal precursor film into a metal oxide one *via* annealing, can be a cost-effective alternative because it can easily form AlO_x at an affordable cost.[18,19] To realize high-performance solution-processed oxide gate dielectrics, several annealing processes have been proposed such as thermal,[20,21] deep ultra-violet (DUV),[22,23] and microwave-assisted annealing,[24] which effectively remove metal ligands and other chemical impurities during metal-oxide framework formation. However, these methods require more than an hour, which is an obstacle to mass production. Therefore, the development of a novel rapid annealing method for metal oxide insulators is indispensable.

The intense pulsed light (IPL) process uses a xenon flash lamp to deliver high energy pulsed light, so that thin films can be rapidly sintered from a precursor film to a metal oxide film. IPL annealing has been applied for metal oxide semiconductor annealing,[25,26] metal ink sintering,[27,28] nanoparticle sintering,[29] and sterilization.[30] However, most studies that apply IPL methods for the formation of metal oxide films have concentrated on semiconductor or electrode variants, with insufficient research on metal oxide gate dielectrics. Recently, several studies have explored the IPL processing method for gate insulators, including notable research studies by Yarali *et al.*[31] and Carlos *et al.*[32] Yarali *et al.* reported solution-processed Al_2O_3/ZrO_2 bilayer dielectric films sintered using IPL, but the dielectric films exhibited low breakdown voltage and high leakage current and are therefore unsuitable for use as a gate insulator. Carlos *et al.* reported the ultrafast combustion synthesis of solution-based AlO_x films using excimer laser

[a]*Division of Nano Convergence Technology Development, Nantional NanoFAB Center, Daejeon, 34141, South Korea*

[b]*Dept. of Electronics Engineering, Chungnam National University, Daejeon, 34134, South Korea. E-mail: gawon@cnu.ac.kr*

[c]*Electronics and Telecommunications Research Institute, 218 Gajeong-ro, Yuseong-gu, Daejeon, 34129, South Korea. E-mail: nkcm@etri.re.kr; Fax: +82-42-860-5202; Tel: +82-42-860-5229*

annealing. The AlO_x film showed suitable breakdown voltage and leakage current with a short processing time. However, this method has the drawback of low large-area uniformity and productivity due to the small laser spot size. Herein, we fabricated a solution-processed AlO_x film by employing IPL annealing. We investigated the effects of IPL on the solution-processed AlO_x film by increasing the number of IPL pulses (P_{IPL}) and analyzed its physical, chemical, and electrical characteristics as a function of P_{IPL}. We demonstrated a rapid manufacturing method using IPL within 30 seconds, which resulted in a dense AlO_x thin film with good electrical characteristics such as high breakdown voltage and low leakage current. Finally, we confirmed that the AlO_x film was suitable to be used as a gate insulator by fabricating indium-gallium-zinc oxide (IGZO) TFTs through the IPL process.

Experimental

Precursor solution synthesis

A 0.6 M aluminum oxide gate dielectric precursor solution was prepared by dissolving aluminum nitrate nonahydrate ($AlN_3O_9 \cdot 9H_2O$, Sigma-Aldrich) in 2-methoxyethanol. The aluminum oxide solution was stirred vigorously at 75 °C for 6 hours under ambient conditions. An IGZO precursor solution was prepared by dissolving indium nitrate nonahydrate ($InN_6O_9 \cdot 9H_2O$, Alfa-Aesar), gallium nitrate hydrate ($GaN_3O_9 \cdot xH_2O$, Sigma-Aldrich), and zinc nitrate hexahydrate ($ZnN_2O_6 \cdot 6H_2O$, Sigma-Aldrich) in 2-methoxyethanol at concentrations of 0.1 M in a molar ratio of 7 : 1.5 : 1.5. The IGZO solution was stirred at 1500 rpm for 6 hours at room temperature. All the precursor solutions were kept under ambient conditions for a day before use.

Thin film fabrication and characterization

Both metal oxide thin films were fabricated on 2 × 2 cm^2 heavily p-doped silicon wafers, which were ultrasonically cleaned in acetone, isopropyl alcohol, and deionized water. To remove the remaining water, the substrates were annealed at 120 °C on a hotplate for 10 min. Next, the substrates were treated with ultraviolet ozone (UVO) for 10 min. The aluminum oxide solution was filtered through a 0.2 μm syringe filter (HP020, Advantec) and then spun on the UVO-treated substrates at 3000 rpm for 60 s. Before IPL irradiation, aluminum oxide precursor thin films were annealed at 100 °C for 10 min under ambient atmosphere to remove the solvents. Thereafter, the AlO_x thin films were irradiated with IPL for 0–450 pulses in the air using xenon flash lamp equipment manufactured by PRO WIN Co., Ltd. The xenon lamp emitted a broad spectrum of light ranging from ultraviolet to infrared region similar to sunlight, covering wavelengths from 200 nm to 2000 nm. The distance between the lamp and the sample was set to 0.5 cm during the IPL process. The frequency and energy of the pulsed light were 15 Hz and 207 J per pulse, respectively. The pulse duration and period were 0.5 ms and 66.7 ms, respectively. The thicknesses of the sol–gel-derived AlO_x films with P_{IPL} were measured using field emission–scanning electron spectroscopy (FESEM, HITACHI SU8230). The average thickness and standard deviation of the AlO_x films were calculated based on three measurement points. The morphologies of the films were characterized through atomic force microscopy (AFM, HORIBA INNOVA-LABRAM HR800) in the tapping mode. X-ray photoelectron spectroscopy (XPS, Thermo VG Scientific Sigma Probe) was employed to obtain the metal–oxygen binding state of the AlO_x dielectric films.

Device fabrication and characterization

To measure insulator properties, an Al electrode (60 nm) was deposited on AlO_x/p^+-Si substrates *via* thermal evaporation. The area of the Al electrode was 500 μm × 500 μm. The capacitance of the dielectric films was measured with a precision LCR meter (HP4284A). The leakage current of the dielectrics and electrical properties of metal–insulator–metal (MIM) devices were measured with a precision semiconductor analyzer (Keithley 4200) in the dark at room temperature. To fabricate IGZO TFTs on AlO_x dielectrics, the 0.1 M IGZO precursor solution was spin-coated on AlO_x at 3000 rpm for 60 s and irradiated with P_{IPL} = 150 × 3. The Al source and drain electrodes were evaporated on the IGZO channel layer. Here, the channel width-to-channel length ratio (W/L) was 7.5 (channel length = 200 μm). The electrical properties of the TFT devices were measured with a semiconductor parameter analyzer (Keithley 4200) in a dark box. Saturation mobility (μ_{sat}) was calculated using the following equation.

$$I_{DS} = \left(\frac{1}{2}\frac{W}{L}\mu_{sat}C_i\right)(V_{GS} - V_{th})^2, \quad (1)$$

where, W and L are the channel width and length of the TFTs, respectively; C_i is the areal capacitance of the AlO_x dielectric; and V_{GS} is the gate-source voltage. Threshold voltage (V_{th}) was determined from measurements in the saturation region by plotting $(I_{DS})^{1/2}$ *vs.* V_{GS} plots. The on/off current ratio (I_{on}/I_{off}) is

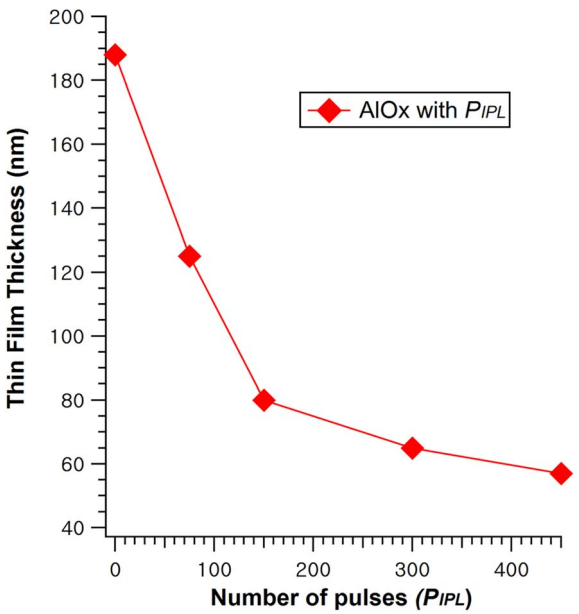

Fig. 1 The thickness of the AlO_x films as a function of P_{IPL}.

often defined as the ratio of the maximum to the minimum drain current. The subthreshold swing (*S.S*) is extracted from the V_{GS} required to increase I_D by a decade through the $(I_{DS})^{1/2}$ *vs.* V_{GS} plots.

Results and discussion

Fig. 1 shows the variation in the of the AlO_x films investigated using FESEM measurements. The thicknesses of AlO_x films irradiated with IPL at 0, 75, 150, 300, and 450 pulses were 188, 125, 80, 65, and 57 nm, respectively. It is clearly observed that the thickness of the film gradually decreases as the P_{IPL} increases, which is due to the reduced residual ligand and solvent as well as the densified metal oxide framework during the IPL-driven decomposition process.[33] The thickness of the controlled film with thermal annealing at 350 °C for 1 hour was 64 nm. Therefore, the AlO_x dielectric film with a P_{IPL} of more than 300 pulses, where the thickness is thinner than 64 nm, is as dense as the thermally annealed film.

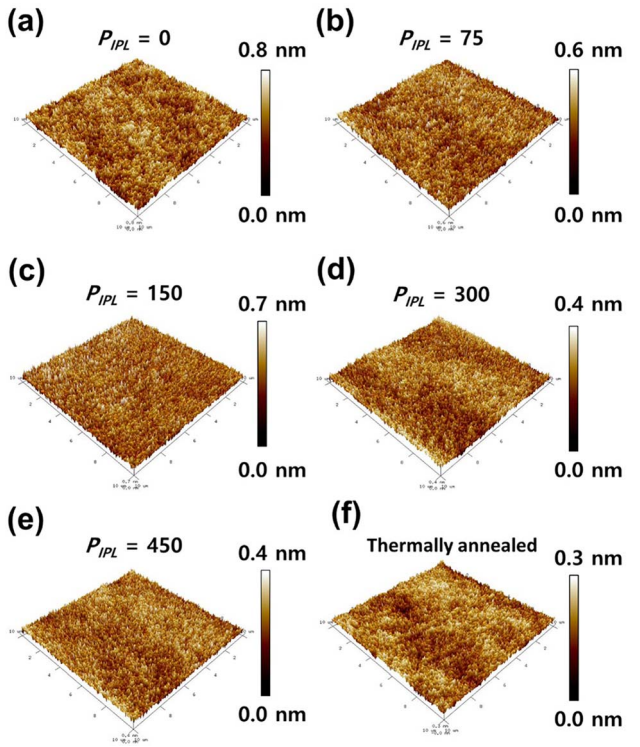

Fig. 2 AFM images of the AlO_x thin film: (a) $P_{IPL} = 0$, (b) $P_{IPL} = 75$, (c) $P_{IPL} = 150$, (d) $P_{IPL} = 300$ (e) $P_{IPL} = 450$, and (f) thermally annealed.

Generally, the surface roughness of a dielectric thin film is critical for charge accumulation at the dielectric/oxide semiconductor interface. The roughness of a dielectric film strongly affects device uniformity and stability. Surface morphologies of the IPL-irradiated AlO_x films were investigated using AFM, as shown in Fig. 2. The root-mean-square roughnesses (R_{RMS}) of the AlO_x film with P_{IPL} values of 0, 75, 150, 300, 450 were 0.21, 0.17, 0.18, 0.11, and 0.11 nm, respectively, which is comparable to that of the thermally annealed film (0.12 nm). The R_{RMS} of the AlO_x thin films tend to decrease as the P_{IPL} increases from 0 to 450 pulses, and this tendency is consistent with that of the film thicknesses mentioned above. Therefore, the high energy of the light makes the exposed films denser and smoother, thus improving device uniformity and stability.

To verify the chemical composition of AlO_x thin films, XPS analysis was carried out. Fig. 3 shows the XPS O 1s spectra of the AlO_x films at different P_{IPL} values, which can be deconvoluted into two peaks: (i) oxygen in metal–oxide–metal (M–O–M) bonds at 531 eV and (ii) oxygen in hydroxide-related (M–OH) bonds at 532.7 eV.[10] The M–O–M and M–OH peaks of the thermally activated AlO_x film are 79% and 21%, respectively. XPS O 1s peaks associated with the M–O–M lattice increase from 1% to 83% and that with the M–OH lattice decreases from 99% to 17% as the P_{IPL} increases from 0 to 450. Before IPL annealing, the remaining metal ligand and solvent in the precursor film contain a number of M–OH bonds, resulting in high M–OH in O 1s XPS spectra. During the annealing process, the M–OH bonds

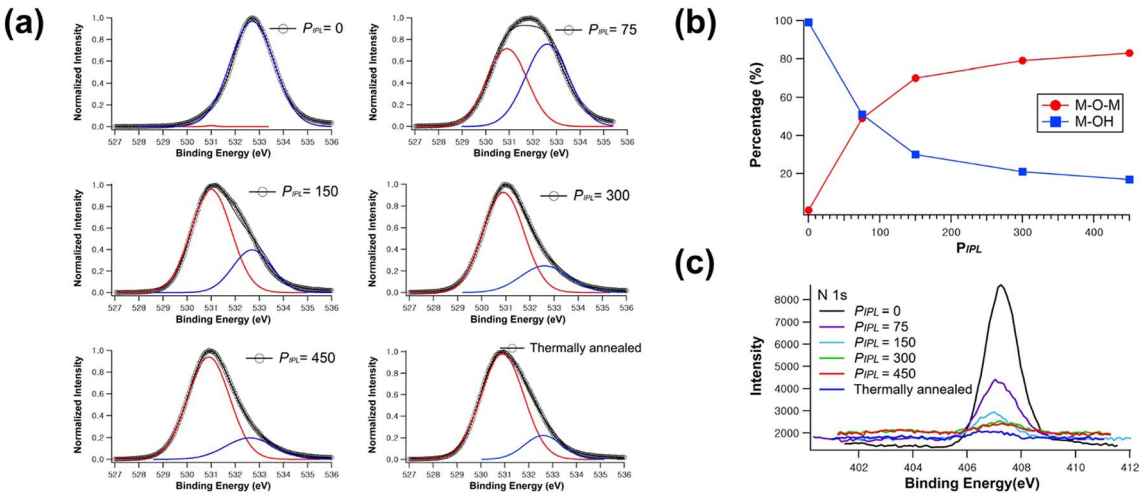

Fig. 3 (a) XPS spectra of O 1s peaks for AlO_x dielectrics with different P_{IPL} values. (b) The variation of oxygen components as a function of P_{IPL}. (c) The corresponding N 1s spectra of the AlO_x thin films.

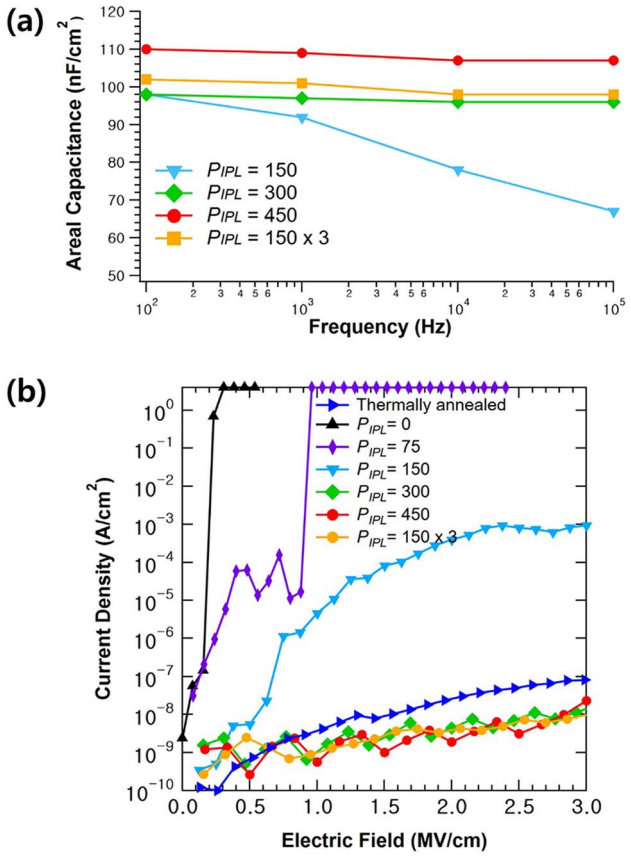

Fig. 4 Electrical characteristics of the solution-processed AlO_x thin film with varying P_{IPL}: (a) capacitance–frequency (C–F) plot. (b) Leakage current density–electric field (J–E) plot.

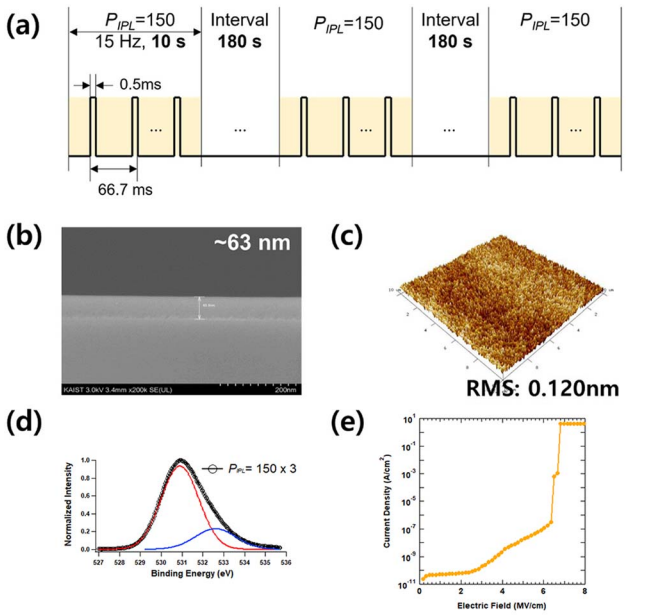

Fig. 5 (a) Schematic of $P_{IPL} = 150 \times 3$. Physical, chemical and electrical properties of AlO_x with $P_{IPL} = 150 \times 3$. (b) Cross-section SEM image. (c) R_{RMS} roughness AFM image, (d) XPS O 1s spectra, and statistical distributions of (e) the J–E plot.

in the film were converted into M–O–M bonds *via* decomposition and densification reactions, thus increasing the M–O–M composition ratio.[34] At P_{IPL} >300, a high composition ratio of the M–O–M bond in the AlO_x films can be achieved, which is comparable to that in thermally annealed AlO_x. Thus, the high concentration of M–O–M bonds indicates that the AlO_x film is properly formed by IPL. Additionally, the residual quantities of nitrogen element within the dielectric layer were also scrutinized to verify metal oxide formation. The disappearance of nitrogen element within the film indicates that IPL irradiation effectively decomposes the aluminum nitrate precursor by eliminating nitrate ligands. As shown in Fig. 3c, the N 1s peak decreases as the irradiation pulse increases. Hence, the XPS data indicate that AlO_x films are properly formed using IPL with a P_{IPL} >300. Note that the frequency of IPL is 15 Hz, which means that the precursor is fully converted into AlO_x within 20 s *via* IPL process, which is much faster than thermal annealing (more than 1 hour).

To characterize the dielectric properties of the AlO_x films irradiated with IPL, a MIM device with a structure of Al/AlO_x/p^+-Si was employed. Fig. 4a shows the capacitance–frequency (C–F) curves of the AlO_x insulators ranging from 100 Hz to 100 kHz. The capacitances for $P_{IPL} = 0$ and 75 at low frequencies could not be measured, likely owing to the resistive characteristics of undecomposed films. The areal capacitance of AlO_x films with a P_{IPL} of 150, 300, and 450 was determined to be 67, 96, and 107 nF cm^{-2} at 100 kHz, respectively, as summarized in Table 1. The

Table 1 Microstructural and dielectric properties of the solution-processed high-κ AlO_x dielectrics with P_{IPL}

Irradiation pulses (P_{IPL})	Thickness (nm)	Roughness (nm)	Capacitance at 100 kHz (nF cm^{-2})	Dielectric constant	Leakage (A cm^{-2}) at 2 mV cm^{-1}
0	188 ± 1.2	0.21	28	—	—
75	125 ± 3.7	0.17	24	—	—
150	80 ± 1.2	0.18	67	—	4.0×10^{-4}
300	65 ± 0.9	0.11	96	7.1	4.4×10^{-9}
450	57 ± 0.5	0.11	107	6.9	1.9×10^{-9}
150 × 3	63 ± 0.5	0.12	98	7.0	4.3×10^{-9}
Thermally annealed	64 ± 7.4	0.12	99	7.2	3.0×10^{-8}

Table 2 Summary of the literature based on photonic-assisted curing metal oxide dielectric films reviewed in this work

References	Material	Processing method	Processing time (min)	Thickness (nm)	Roughness (nm)	Dielectric constant (k)	Breakdown field (MV cm^{-1})	Leakage current density at 2 MV cm^{-1} (A cm^{-2})
22	Al_2O_3	DUV	120	47	0.226	8	>6	$\sim 1 \times 10^{-8}$
30	ZrO_2/Al_2O_3	IPL	≤1	30	0.430	—	1	$<1 \times 10^{-5}$ at 1 MV cm^{-1}
31	AlO_x	Excimer laser	≤1	15	2.8	~9	4	$\sim 1 \times 10^{-6}$
38	AlO_x	UV + thermal	140	50	0.260	6–8	5.1	$\sim 5 \times 10^{-6}$ at 1 MV cm^{-1}
39	$AlO_x/YAlO_x$	DUV	165	30	—	~10	—	—
This work	AlO_x	IPL	≤1	63	0.120	7	>6	4.3 × 10−9

relatively low capacitance of the AlO_x film with a P_{IPL} of less than 150 can be attributed to imperfect M–O–M bonds, which result from undecomposed residuals and remaining solvent. Besides, capacitance tends to rapidly decrease as frequency increases. When the P_{IPL} is > 300, capacitance changes in the AlO_x film with respect to frequency are insignificant, caused by much lower residual impurities such as M–OH and nitrogen elements.[35] The dielectric constant of a solution-processed AlO_x insulator was calculated using the following formula.

$$C = \varepsilon_0 \varepsilon_r \frac{A}{d}, \quad (2)$$

where C is the capacitance, A is the contact area, d is the thickness of the gate dielectric layer, ε_0 is vacuum permittivity, and ε_r is the dielectric constant. Using eqn (2), the dielectric constants of the AlO_x insulator with P_{IPL} values of 300 and 450 were calculated to be approximately 7, which corresponds to that of the thermally-annealed solution-processed AlO_x film (6–7).[11]

Fig. 4b shows the leakage current density–electric field (J–E) characteristics of AlO_x films as a function of P_{IPL}. In the case of AlO_x with $P_{IPL} \leq 150$, its leakage current density was measured to be more than 10^{-4} A cm^{-2} at 2 MV cm^{-1}, making it difficult to use as a gate insulator. It is known that the leakage current of a film should be lower than 10^{-6} A cm^{-2} to employ it as a gate insulator.[36] On increasing the irradiation pulses from 150 to 450, leakage current is reduced to less than 10^{-8} A cm^{-2} at 2 MV cm^{-1}, which is comparable to that of previously reported solution-processed gate insulators.[37–39] As mentioned earlier, these excellent dielectric properties of IPL-annealed AlO_x can be attributed to the formation of high-composition M–O–M bonds during high-energy pulse irradiation, which can improve the frequency dependence of capacitance.

As the IPL irradiation pulse increases, dielectric properties, such as leakage current, capacitance, and roughness, of the thin film enhanced. A P_{IPL} of 450 is an optimum condition for forming the AlO_x film with low leakage current and high capacitance. However, continuous pulsed light irradiation can cause substrate overheating, which can be a problem in the case of plastic substrates because of thermal expansion mismatch and deformation. Our previous research showed that substrate temperatures after the IPL process at P_{IPL} = 75, 150, 300, and 450 were measured to be 131.5 °C, 205.8 °C, 272.8 °C and 297.0 °C, respectively.[25] Therefore, to keep substrate temperature below 200 °C while maintaining the total irradiation, a P_{IPL} of 150 was irradiated three times with an interval of 3 min. Fig. 5a shows a schematic of the $P_{IPL} = 150 \times 3$. To confirm the dielectric integrity of the AlO_x film with $P_{IPL} = 150 \times 3$, the physical, chemical and electrical properties of the film and MIM device were fully characterized. The SEM and AFM images of the dielectric film with $P_{IPL} = 150 \times 3$ are shown in Fig. 5a and b. The thickness of the AlO_x film is approximately 60 nm, and its surface morphology exhibits a uniform surface with an R_{RMS} value of 0.120 nm. As shown in Fig. 5c, the M–O–M and M–OH lattice peaks were determined to be 80% and 20%, respectively. From physical and chemical analysis, it is considered that the IPL irradiation of $P_{IPL} = 150 \times 3$ transfers enough energy to form a dense AlO_x film, comparable to the thermally annealed AlO_x film and P_{IPL} = 450-irradiated one. To verify the electrical characteristics of AlO_x with $P_{IPL} = 150 \times 3$, the breakdown field and leakage current density are presented in Fig. 5d. The electrical properties of the MIM devices exhibit low leakage current (<10^{-8} A cm^{-2} at 2 MV cm^{-1}) and high breakdown field (>6 MV cm^{-1}). Note that because the operating field of typical TFTs is −3 MV cm^{-1}–+3 MV cm^{-1}, the TFT employing the AlO_x film with $P_{IPL} = 150 \times 3$, annealed within only 30 s under ambient

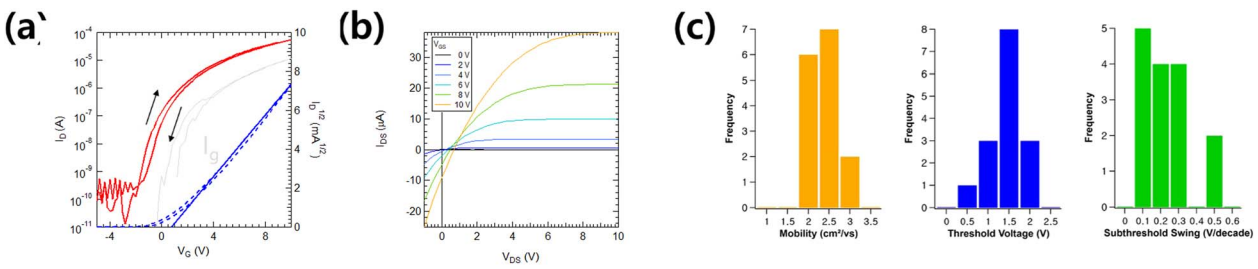

Fig. 6 All-solution-processed and entirely IPL irradiation metal oxide devices. (a) Double-sweep transfer curves, (b) output curves, and (c) statistical distributions of the field-effect mobility, threshold voltage, and subthreshold swing of AlO_x/IGZO TFTs with $P_{IPL} = 150 \times 3$.

conditions, could be properly operated without breakdown. Table 2 summarizes the properties of AlO_x dielectric films fabricated through various photonic-assisted processing methods. Compared to films reported in previous studies, the film achieved in this study demonstrates both superior electrical properties, such as a high breakdown field (>6 MV cm^{-1}) and low leakage current (<10^{-8} A cm^{-2} at 2 MV cm^{-1}), as well as a short processing time (<1 min).

To evaluate the feasibility of the AlO_x dielectric film with $P_{IPL} = 150 \times 3$, solution-processed metal oxide TFTs were fabricated using AlO_x gate dielectrics and IGZO semiconducting layer irradiated with IPL on the p^{++} Si substrate. The transfer characteristic of the IGZO TFT with the IPL process is shown in Fig. 6a. The transfer curves of the IGZO/AlO_x TFT exhibits a μ_{sat} of 2.99 cm^2 V^{-1} s^{-1}, V_{th} of 0.73 V, and I_{on}/I_{off} ratio of 3.9×10^6. Generally, hysteresis may be related to charge trapping/detrapping behavior at the semiconductor/dielectric interface. For AlO_x/IGZO TFTs, transfer curves with lower hysteresis properties are possibly due to the smooth surface roughness and high M–O–M conversion ratio. From statistical data, averaged values over 15 IGZO/AlO_x devices indicate a highly uniform distribution, as shown in Fig. 6b. Note that the electrical performance with a μ_{sat} of 2.31 cm^2 V^{-1} s^{-1} and low hysteresis of the IGZO/AlO_x TFTs demonstrates that excellent interfacial properties and a high-quality sol–gel oxide film structure can be obtained *via* rapid activation with $P_{IPL} = 450$ despite a short irradiation time (<30 seconds). This result attests that the rapid activation process enabled the conversion of the solution-processed oxide-based materials into highly stable and reliable gate dielectrics and semiconductors.

Conclusion

In summary, we present a novel IPL annealing method for the rapid activation of a solution-processed high-κ dielectric film. When the AlO_x film was formed by irradiating IPL in the range of 0–450, the thickness of the dielectric thin film tended to decrease from 188 nm to 57 nm. Likewise, AFM analysis of AlO_x with P_{IPL} represents a flat surface roughness of ≤0.2 nm. When the aluminum precursor film was irradiated with IPL for ≥300 pulses, XPS analysis shows that the M–O–M bond ratio was 80%, and residual amounts of nitrogen element were effectively removed, indicating that the decomposition and densification reactions occurred as the IPL irradiation pulse increased. The resulting AlO_x dielectric film at $P_{IPL} = 450$ exhibits high electrical performance, including a large area-capacitance of 109 nF cm^{-2} and low leakage current density of <10^{-8} A cm^{-2} at 2 MV cm^{-1}. In order to prevent the lamp from overheating, an AlO_x thin film was formed at $P_{IPL} = 150 \times 3$. The optimized AlO_x/IGZO TFTs with $P_{IPL} = 150 \times 3$ exhibit a μ_{sat} of 2.99 cm^2 V^{-1} s^{-1}, V_{th} of 0.73 V, *S.S* of 180 mV per decade, I_{on}/I_{off} of 3.9×10^6, and low operating voltage of 10 V. Herein, AlO_x dielectric thin film with P_{IPL} was fabricated under simple, ambient conditions and at low cost. Thus, the comprehensive investigation of their spectroscopic analysis and electrical properties demonstrates their potential as a promising high-κ dielectric for low-voltage high-performance oxide TFT devices. It is expected that the results obtained in this research can be widely used in the application of gate dielectric layers for metal oxide electronic devices.

Data availability

The data supporting the findings of this study are available within the article.

Conflicts of interest

There are no conflicts to declare.

Acknowledgements

This work was partially supported by the Technology Innovation Program (RS-2023-00257784, RS-2024-00417392) funded by the Ministry of Trade, Industry & Energy (MOTIE), Electronics and Telecommunications Research Institute (ETRI) grant funded by the Korea government (21ZB1200, The Development of the Technologies for ICT Materials, Components and Equipment).

References

1 Y. You, J. Lim, K. Son, J. Kim, K. Lee, K. Chung and K. Park, *Electronics*, 2024, **13**, 2254.
2 B. Park, S. Nam, Y. Kang, S. Jeon, J. W. Jo, S. K. Park and Y. H. Kim, *Mater. Today Electron.*, 2024, **8**, 100090.
3 R. Shi, Y. Wang, Z. Xia and M. Wong, *IEEE Trans. Electron Devices*, 2023, **70**, 5140.
4 W. Kim, S. Kang, Y. Lee, S. Mun, J. Choi, S. Lee and C. S. Hwang, *J. Mater. Chem. C*, 2023, **11**, 8254–8262.
5 S. R. Bhalerao, D. Lupo and P. R. Berger, *Mater. Sci. Semicond. Process.*, 2022, **139**, 106354.
6 W. S. Cheong, Y. H. Kim, J. M. Lee, C. H. Hong, H. Y. Choi, Y. J. Kwak, Y. J. Kim and Y. S. Kim, *Adv. Mater. Technol.*, 2019, **4**, 1800550.
7 B. H. Lee, L. Kang, R. Nieh, W.-J. Qi and J. C. Lee, *Appl. Phys. Lett.*, 2000, **76**, 1926.
8 M. S. Oh, K. Lee, J. Song, B. H. Lee, M. M. Sung, D. Hwang and S. Im, *J. Electrochem. Soc.*, 2008, **155**, H1009.
9 J. H. Park, Y. B. Yoo, K. H. Lee, W. S. Jang, J. Y. Oh, S. S. Chae and H. K. Baik, *ACS Appl. Mater. Interfaces*, 2013, **5**, 410.
10 J. W. Jo, J. Kim, K. T. Kim, J. G. Kang, M. G. Kim, K. H. Kim, H. Ko, Y. H. Kim and S. K. Park, *Adv. Mater.*, 2015, **27**, 1182.
11 I. M. Jauhari, Y. G. Bak, I. Noviyana, M. A. Putri, J. A. Lee, Y. W. Heo, H. Y. Lee and J. Nanosci, *Nanotechnol*, 2021, **21**, 1748.
12 M. L. Lee, C. H. Kao, H. Chen, C. Y. Lin, Y. T. Chung and K. M. Chang, *Ceram. Int.*, 2017, **43**, 3043.
13 S. A. K. M. Faruque, D. Debnath, B. Giri and S. Chakraborty, *J. Cryst. Growth*, 2017, **459**, 38.
14 I. Fina and F. Sanchez, *ACS Appl. Electron. Mater.*, 2021, **3**, 1530–1549.
15 X. Y. Zhang, J. Han, D. C. Peng, Y. J. Ruan, W. Y. Wu, D. S. Wuu, C. J. Huang, S. Y. Lien and W. Z. Zhu, *Nanomaterials*, 2022, **12**, 3890.

16 P. Li, J. Yang, X. Ding, X. Li and J. Zhang, *IEEE J. Electron Devices Soc.*, 2024, **12**, 121.
17 T. E. Taouririt, A. Meftah and N. Senouga, *Appl. Nanosci.*, 2018, **8**, 1865.
18 W. Xu, H. Wang, L. Ye and J. Xu, *J. Mater. Chem. C*, 2014, **2**, 5389.
19 L. Zhang, Q. Zhang, G. Xia, J. Zhou and S. Wang, *J. Mater. Sci.: Mater. Electron.*, 2015, **26**, 6639.
20 W. Xu, H. Wang, F. Xie, J. Chen, H. Cao and J.-B. Xu, *ACS Appl. Mater. Interfaces*, 2015, **7**, 5803.
21 Y. Su, C. Wang, W. Xie, F. Xie, J. Chen, N. Zhao and J. Xu, *ACS Appl. Mater. Interfaces*, 2011, **3**, 4662.
22 B. S. Yu, J. Y. Jeon, B. C. Kang, W. B. Lee, Y. H. Kim and T. J. Ha, *Sci. Rep.*, 2019, **9**, 8416.
23 J. W. Jo, J. Kim, K. T. Kim, J. G. Kang, M. G. Kim, K. H. Kim, H. Ko, Y. H. Kim and S. K. Park, *Adv. Mater.*, 2015, **27**, 1182.
24 S. Wang, S. Yao, J. Lin and G. Xia, *Ceram. Int.*, 2019, **45**, 9829.
25 D. W. Kim, J. Park, J. Hwang, H. D. Kim, J. H. Ryu, K. B. Lee, K. H. Baek, L.-M. Do and J. S. Choi, *Electron. Mater. Lett.*, 2015, **11**, 82.
26 C.-M. Kang, H. Kim, Y.-W. Oh, K.-H. Baek and L.-M. Do, *IEEE Electron Device Lett.*, 2016, **37**, 595.
27 H.-S. Kim, S. R. Dhage, D.-E. Shim and H. T. Hahn, *Appl. Phys. A: Mater. Sci. Process.*, 2009, **97**, 791.
28 H. Kang, E. Sowade and R. R. Baumann, *ACS Appl. Mater. Interfaces*, 2014, **6**, 1682.
29 J. Niittynen, E. Sowade, H. Kang, R. R. Baumann and M. Mäntysalo, *Sci. Rep.*, 2015, **5**, 8832.
30 J. J. Baek, S. M. Park, Y. R. Kim, K. C. Chang, Y. J. Heo, G. Y. Bae, K. H. Choi and G. Shin, *J. Mater. Sci.*, 2022, **57**, 254.
31 E. Yarali and T. D. Anthopoulos, *Adv. Electron. Mater.*, 2020, **6**, 200028.
32 E. Carlos, S. Dellis, N. Kalfagiannis, L. Koutsokeras, D. C. Koutsogeorgis, R. Branquinho, R. Martins and E. Fortunato, *J. Mater. Chem. C*, 2020, **8**, 6176.
33 R. Branquinho, D. Salgueiro, L. Santos, P. Barquinha, L. Pereira, R. Martins and E. Fortunato, *ACS Appl. Mater. Interfaces*, 2014, **6**, 19592.
34 S. Y. Je, B.-G. Son, H.-G. Kim, M.-Y. Park, L.-M. Do, R. Choi and J. K. Jeong, *ACS Appl. Mater. Interfaces*, 2014, **6**, 18693.
35 K. Banger, C. Warwick, J. Lang, K. Broch, J. E. Halpert, J. Socratous, A. Brown, T. Leedham and H. Sirringhaus, *Chem. Sci.*, 2016, **7**, 6337.
36 J. H. Park, S. J. Lee, T. I. Lee, J. H. Kim, C.-H. Kim, G. S. Chae, M.-H. Ham, H. K. Baik and J.-M. Myoung, *J. Mater. Chem. C*, 2013, **1**, 1840.
37 S. Park, K. H. Kim, J. W. Jo, S. Sung, K. T. Kim, W. J. Lee, J. Kim, H. J. Kim, G. R. Yi and Y. H. Kim, *Adv. Funct. Mater.*, 2015, **25**, 2807.
38 W. J. Scheideler, M. W. McPhail, R. J. Kumar, J. Smith and V. Subramanian, *ACS Appl. Mater. Interfaces*, 2018, **10**, 37277.
39 A. Mancinelli, S. Bolat, J. Kim, Y. E. Romanyuk and D. Briand, *ACS Appl. Electron. Mater.*, 2020, **2**, 3141.